Green Chemistry

PAPER

View Article Online
View Journal | View Issue

Cite this: *Green Chem.*, 2024, **26**, 936

Manufacture of olefins by the selective hydrodeoxygenation of lignocellulosic ketones over a cobalt molybdate catalyst†

Fengan Han,[a,b,c] Guangyi Li,[a] Yanting Liu,[a] Aiqin Wang,[a,d] Feng Wang,[d] Tao Zhang[a,b,d] and Ning Li *[a]

Olefins are important feedstocks in the production of fuels and many useful chemicals. Herein, cobalt molybdate ($CoMoO_4$) was first synthesized by an environmentally friendly evaporation method and it exhibited excellent catalytic performance for the production of olefins by the selective hydrodeoxygenation (HDO) of ketones that can be derived from lignocellulose. On the basis of the characterization results, the excellent catalytic performance of $CoMoO_4$ was attributed to its larger specific surface area, better pore structure, higher oxygen vacancy (or Mo^{5+} species) concentration, higher acid strength and higher concentration of acid sites. Under the optimized reaction conditions, 4-heptanone was almost completely converted to heptene, and a high carbon yield of heptene (96%) was achieved over a $CoMoO_4$ catalyst with a Co/Mo atomic ratio of 0.8 (denoted as $CoMoO_4$-0.8). The $CoMoO_4$ catalyst is also active for the selective HDO of other lignocellulosic ketones (such as acetone, butanone, 2-pentanone, 3-pentanone, cyclopentanone, cyclohexanone, 5-nonanone and acetophenone) to their corresponding olefins.

Received 9th October 2023,
Accepted 11th December 2023

DOI: 10.1039/d3gc03825d

rsc.li/greenchem

Introduction

Due to the great social concerns about the environmental and sustainable development issues, the utilization of renewable energy has emerged as a hot research topic. As the main component of agricultural and forestry waste, lignocellulose is a cheap and abundant carbon resource.[1,2] In recent years, the catalytic conversion of lignocellulose to hydrogen, methane, liquid biofuels and value-added chemicals has aroused widespread concern.[3,4]

Olefins are basic feedstocks in the production of fuels, lubricants, drugs, cosmetics, polymers, coatings, surfactants, detergents, *etc.*[5] Traditionally, olefins are mainly obtained by dehydrogenation of alkanes, metathesis, catalytic cracking and pyrolysis from nonrenewable petrochemical resources.[6] The manufacturing procedure of olefins is generally energy-intensive and leads to a significant amount of CO_2 emission.[7] From a long-term perspective, it is still imperative to develop a highly integrated method for the manufacture of olefins with lignocellulose-derived feedstocks.

Ketones are a class of oxygenated hydrocarbons that can be obtained from lignocellulose by fermentation or catalytic conversion. For instance, acetone, as a useful chemical, can be obtained from the fermentation of lignocellulose by an acetone–butanol–ethanol (ABE) method.[8] Apart from this, the ketonization reaction of acetic acid obtained from the production of furfural as a by-product can be used to manufacture acetone.[9] Butanone can be synthesized by the decarboxylation reaction of levulinic acid.[10] Using a bi-metallic Cu–Ni/SBA-15 catalyst, 2-pentanone can be derived from the hydrogenolysis of furfural.[11] Meanwhile, the catalytic conversion of ABE fermentation products is another method to produce 2-pentanone.[2] 3-Pentanone can be obtained from the ketonization of propionic acid, which is the partial HDO product of lactic acid[12] obtained from the chemical or biological degradation of cellulose.[13] Cyclopentanone can be obtained from the aqueous-phase selective hydrogenation of furfural.[14] Cyclohexanone is the product of hydrogenation of phenol[15] which can be obtained from lignin. The ABE fermentation product can be converted to 4-heptanone by tin-doped ceria catalysts.[16] As the partial HDO product of levulinic acid, valeric acid can be converted into 5-nonanone by ketonization.[17] Acetophenone, as a representative of aromatic ketones, can be derived from lignin.[18] The selective hydrodeoxygenation (HDO) of these ketones to obtain the corresponding olefins by a one-step reaction has great significance.

[a]*CAS Key Laboratory of Science and Technology on Applied Catalysis, Dalian Institute of Chemical Physics, Chinese Academy of Sciences, Dalian 116023, China. E-mail: lining@dicp.ac.cn*
[b]*Department of Chemical Physics, School of Chemistry and Materials Science, University of Science and Technology of China, Hefei 230026, China*
[c]*University of Chinese Academy of Sciences, 19 A Yuquan Road, Shijingshan District, Beijing 100049, China*
[d]*State Key Laboratory of Catalysis, Dalian Institute of Chemical Physics, Chinese Academy of Sciences, Dalian 116023, China*

† Electronic supplementary information (ESI) available. See DOI: https://doi.org/10.1039/d3gc03825d

Cobalt molybdate ($CoMoO_4$) is a low cost, non-toxic and abundant molybdate that has a wide range of applications in electrocatalysis,[19] energy storage materials[20] and catalytic oxidation.[21] Generally, $CoMoO_4$ is obtained by a co-precipitation method,[22] a hydrothermal method[19,20] and a sol–gel method.[21] These methods are relatively complicated and environmentally unfriendly. In this work, a $CoMoO_4$ catalyst was first manufactured by a simple and environmentally friendly evaporation method and it demonstrated excellent activity for the selective HDO of lignocellulose-derived ketones to olefins. Under the optimal reaction conditions (673 K, 0.1 MPa H_2, WHSV = 10 h^{-1}, H_2/4-heptanone molar ratio = 50 : 1), the conversion of 4-heptanone and the carbon yield of heptene could reach 98% and 96%, respectively. According to the characterization results, it was found that the excellent catalytic activity of $CoMoO_4$ was attributed to its larger specific surface area, good pore structure, higher oxygen vacancy (or Mo^{5+} species) concentration, stronger acidity and higher acid site concentration. Furthermore, cobalt molybdate catalysts also exhibited excellent catalytic activity for the selective HDO of other lignocellulosic ketones (such as acetone, butanone, 2-pentanone, 3-pentanone, cyclopentanone, cyclohexanone, 5-nonanone and acetophenone) to their corresponding olefins (propylene, butene, pentene, cyclopentene, cyclopentadiene, cyclohexene, styrene and nonene). The strategy of our work is shown in Fig. 1.

Experimental

Chemicals

Cobalt oxide (CoO), cobalt nitrate hexahydrate ($Co(NO_3)_2{\cdot}6H_2O$, AR), copper nitrate trihydrate ($Cu(NO_3)_2{\cdot}3H_2O$, AR), iron nitrate nonahydrate ($Fe(NO_3)_3{\cdot}9H_2O$, 99.9%), nickel nitrate hexahydrate ($Fe(NO_3)_2{\cdot}6H_2O$, AR) and internal standard substances (such as dodecane, 1,4-dioxane and cyclohexanone) were supplied by Shanghai Aladdin Bio-Chem Technology Co., Ltd. Ammonium molybdate tetrahydrate ($(NH_4)_6Mo_7O_{24}{\cdot}4H_2O$, AR) was purchased from Meryer (Shanghai) Chemical Technology Co. Ethanol (AR) and methanol (AR) were supplied by Shanghai Sinopharm Chemical Reagent Co., Ltd.

Catalyst preparation

The MoO_3 catalyst was manufactured by the calcination of $(NH_4)_6Mo_7O_{24}{\cdot}4H_2O$ at 873 K for 2 h. The MoO_3 + CoO catalyst was obtained by physically mixing MoO_3 and CoO at a molar ratio of 1 : 1. The $CoMoO_4$ catalyst was synthesized by a modified evaporation method.[23] First, 4 mmol of $(NH_4)_6Mo_7O_{24}{\cdot}4H_2O$ and 28 mmol of $Co(NO_3)_2{\cdot}6H_2O$ were dissolved in 200 mL of water. The mixture was heated at 373 K to remove the water by evaporation. The product was calcined at 673 K for 2 h. For comparison, we also prepared a MoO_3/CoO catalyst (with a Co/Mo atomic ratio of 1 : 1) by an impregnation method.[24] Furthermore, the other molybdate catalysts ($Fe_2(MoO)_3$, $CuMoO_4$, and $NiMoO_4$) were synthesized by the same evaporation method.

Characterization

The X-ray diffraction (XRD) spectra of the catalysts were obtained using a PW3040/60X' Pert PRO (PANAlytical) diffractometer.

The scanning electron micrograph (SEM) images of the samples were acquired using a JSM-7800F field-emission SEM device to analyze the morphology. The transmission electron microscopy (TEM) images of the samples were acquired from a JEM-2100F field emission electronic microscope to analyze the morphology and composition.

The N_2-physisorption of the catalysts was performed using Micromeritics ASAP 2010 apparatus. Before the tests, the samples were evacuated for 6 h to eliminate the adsorbents.

The H_2-temperature programmed reduction (H_2-TPR) of the catalysts was conducted using a Micromeritics AutoChem II 2920 Characterization System. Before the tests, the samples were pretreated for 0.5 h under Ar flow at 673 K to remove the

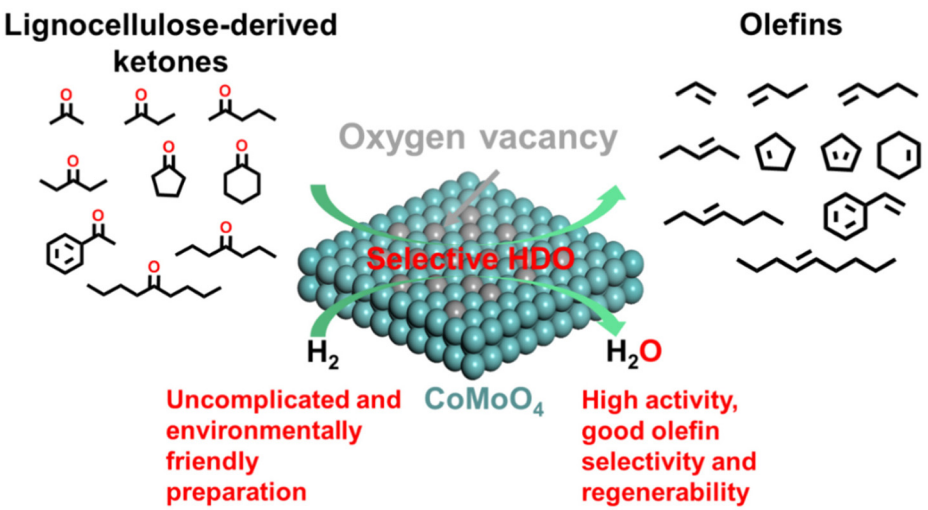

Fig. 1 Strategy for the production of olefins from lignocellulose-derived ketones over the $CoMoO_4$ catalyst.

impurities that were adsorbed on the surface of the samples. After being cooled down to 333 K under the Ar flow, the catalysts were heated from 333 K to 1073 K at a rate of 10 K min^{-1} under 10% H_2/Ar flow. After the removal of water by a cold trap at the outlet of the reactor, the hydrogen consumed in the measurement was detected using a thermal conductivity detector (TCD).

The NH_3-temperature programmed desorption (NH_3-TPD) of the catalysts was conducted using a Micromeritics AutoChem II 2920 Characterization System. First, the catalysts were pretreated at 673 K for 1 h under H_2 flow (as we did for activity tests) and cooled down to 373 K under He flow. After NH_3 adsorption saturation at 373 K, the desorption of NH_3 was conducted from 373 K to 1173 K (at a rate of 10 K min^{-1}). The desorbed NH_3 was detected using an OminiStar mass spectrometer.

The X-ray photoelectron spectroscopy (XPS) of catalysts was conducted using a Thermo Fisher ESCALAB 250Xi.

The ultraviolet-visible (UV-Vis) diffuse reflectance spectroscopy of catalysts was performed using a PerkinElmer Lambda 950 UV/Vis/NIR spectrometer.

The online-tandem thermogravimetric-mass spectrometry (TG-MS) analysis was conducted using a TA Instruments SDT Q600 connected with an OminiStar mass spectrometer to monitor the formation of gaseous products during the test from 298 K to 1273 K (with a ramp of 10 K min^{-1}) under air.

Activity test

The selective HDO of lignocellulose-derived ketones was conducted using a fixed-bed reactor described in our previous work.[24] Prior to the activity test, the catalysts were reduced under H_2 flow for 1 h at 673 K. Subsequently, the ketones were pumped into the tubular reactor using a HPLC pump. After passing the reactor, the products were cooled down and separated by a cold trap, the gaseous products were analyzed using an on-line Agilent 6890N GC, and the liquid products were gathered in the cold trap and analyzed using an Agilent 7890A GC after 5 h. The conversions of the substrates and the carbon yields of specific products were calculated using the following equations:

$$\text{Conversion of the ketones}(\%) = (\text{molar of the ketones consumed during activity test})/(\text{molar of the ketones in the feedstock}) \times 100\%.$$

$$\text{Carbon yield of specific product}(\%) = (\text{molar of carbon the specific product obtained inactivity evaluation})/(\text{molar of carbon the ketones in the feedstock}) \times 100\%.$$

Results and discussion

Characterization

Based on the morphologies of the MoO_3, CoO, MoO_3/CoO and $CoMoO_4$ catalysts (shown in Fig. 2 and 3), the MoO_3 catalyst has an irregular structure, while the CoO catalyst mainly consists of a nanoparticle structure. Different from MoO_3 and CoO, the MoO_3/CoO obtained by the impregnation method has a nanorod structure. The $CoMoO_4$ manufactured by the evaporation method has a disordered nano-scale particle stacking structure. According to the STEM-EDX results of MoO_3/CoO and $CoMoO_4$ (Fig. 4), the Co, Mo and O species were evenly distributed in the surfaces of the MoO_3/CoO and $CoMoO_4$ catalysts. The surface Co/Mo atomic ratios of the MoO_3/CoO and $CoMoO_4$ catalysts were found to be 0.99 and 0.94, respectively. These values are consistent with the theoretical Co/Mo atomic ratios in the MoO_3/CoO and $CoMoO_4$ catalysts (*i.e.* 1 : 1).

The specific BET surface areas (S_{BET}), pore volumes and average pore diameters of the CoO, MoO_3, MoO_3/CoO and $CoMoO_4$ catalysts were analyzed by N_2-physisorption. According to Table 1 and Fig. S1,† the S_{BET} values of CoO (9.9 m^2 g^{-1}), MoO_3 (2.4 m^2 g^{-1}) and MoO_3/CoO (7.7 m^2 g^{-1})

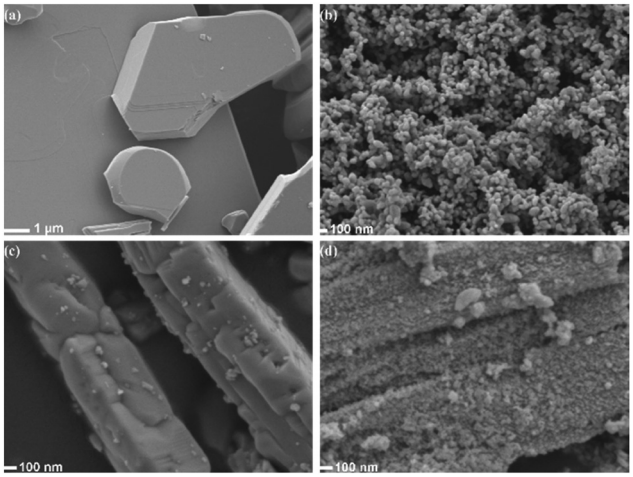

Fig. 2 SEM images of the (a) MoO_3, (b) CoO, (c) MoO_3/CoO and (d) $CoMoO_4$ catalysts.

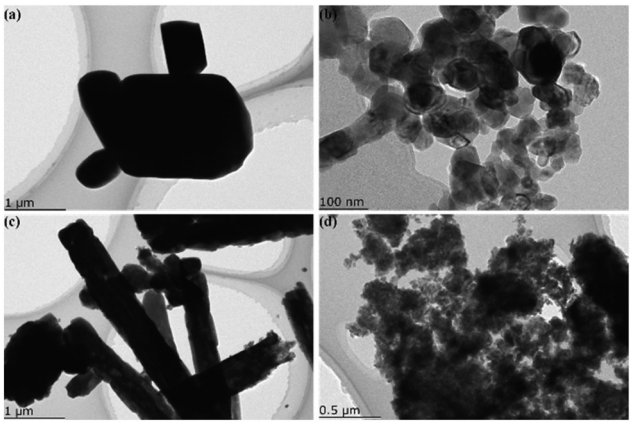

Fig. 3 STEM images of the (a) MoO_3, (b) CoO, (c) MoO_3/CoO and (d) $CoMoO_4$ catalysts.

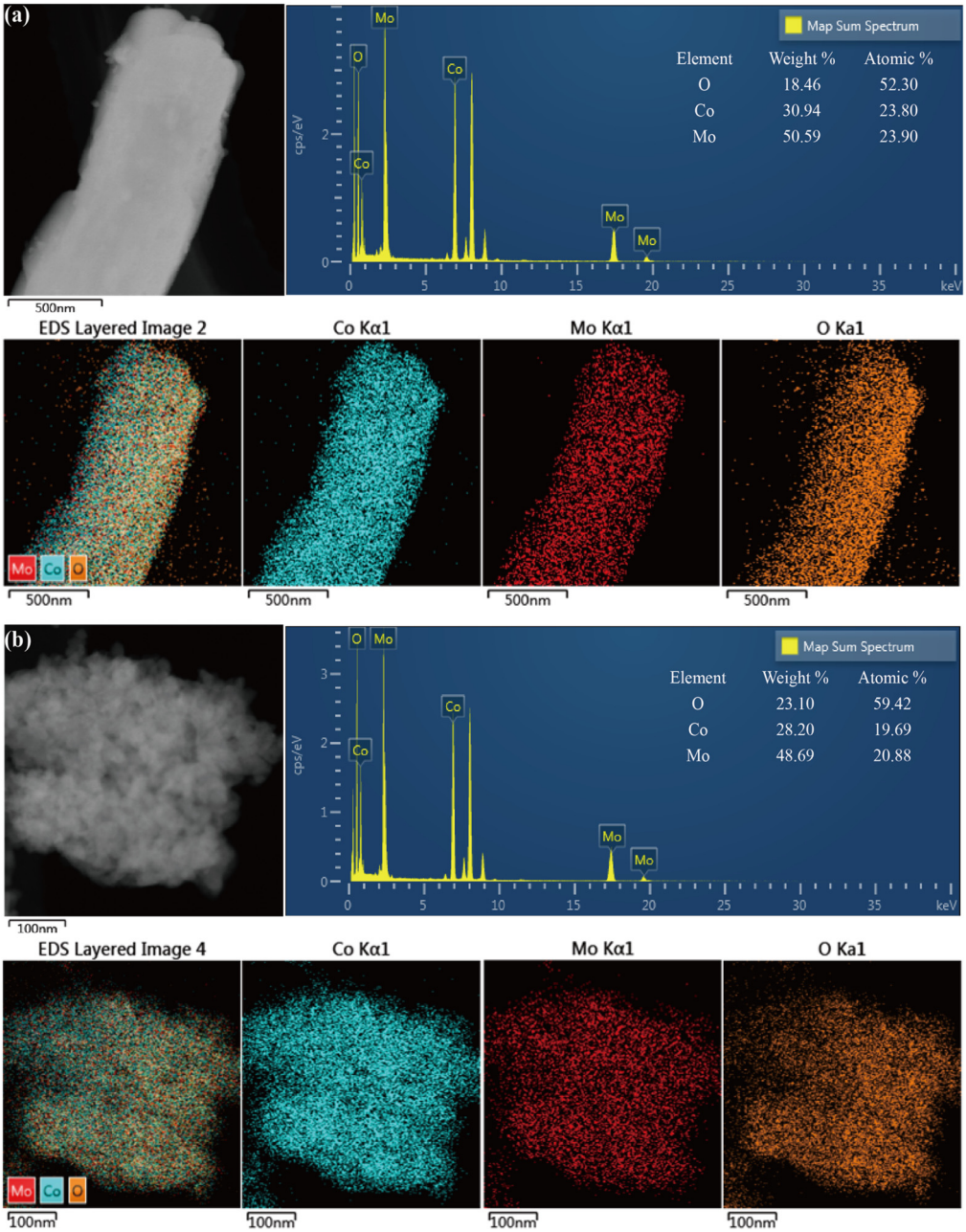

Fig. 4 TEM-EDX elemental mapping images of the (a) MoO_3/CoO and (b) $CoMoO_4$ catalysts.

are smaller than that of $CoMoO_4$ (22.1 m^2 g^{-1}). Furthermore, the pore volume and average pore diameter of $CoMoO_4$ are greater than those of MoO_3/CoO and CoO.

Table 1 The specific BET surface areas (S_{BET}), pore volumes and average pore sizes of the CoO, MoO_3, MoO_3/CoO and $CoMoO_4$ catalysts

Catalyst	S_{BET} (m^2 g^{-1})	Pore volume (μL g^{-1})	Average pore size (nm)
CoO	9.9	15.2	6.8
MoO_3	2.4	2.3	6.1
MoO_3/CoO	7.7	22.5	10.4
$CoMoO_4$	22.1	101.6	17.8

According to the XRD diffraction results illustrated in Fig. 5, the MoO_3 manufactured by the calcination method is mainly composed of an orthorhombic MoO_3 phase (PDF#05-0508). The CoO supplied by Shanghai Aladdin Bio-Chem Technology is mainly composed of a CoO phase with a cubic crystal structure (PDF#48-1719). The MoO_3/CoO synthesized by the impregnation method is mainly composed of a monoclinic $CoMoO_4$ phase (PDF#21-0868). The $CoMoO_4$ obtained by the evaporation method exists in a monoclinic $CoMoO_4$ phase (PDF#21-0868). After reduction under hydrogen flow at 673 K for 1 h, no significant change was observed in the XRD pattern of the MoO_3 catalyst (see Fig. 6). In contrast, a metallic Co phase (PDF#05-0727) was generated by the reduction of CoO

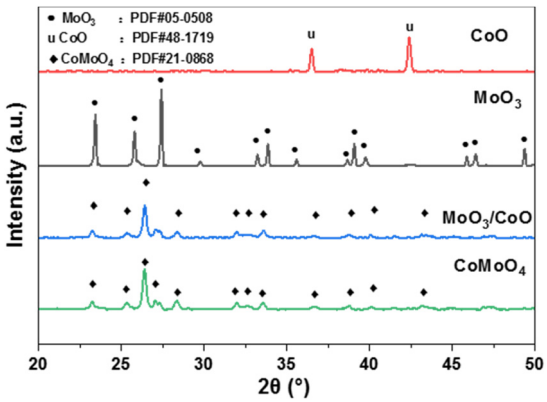

Fig. 5 XRD patterns of the MoO_3, CoO, MoO_3/CoO and $CoMoO_4$ catalysts.

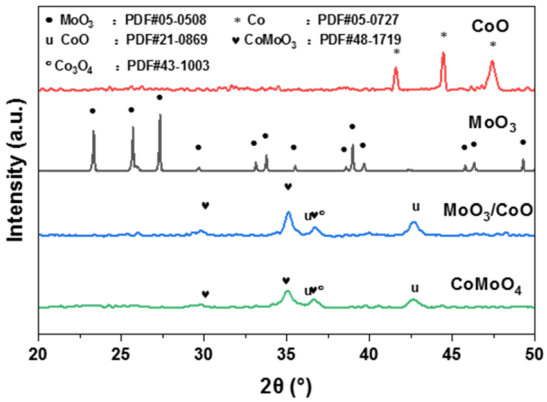

Fig. 6 XRD patterns of the reduced MoO_3, CoO, MoO_3/CoO and $CoMoO_4$ catalysts.

by H_2. The MoO_3/CoO and $CoMoO_4$ catalysts were transformed from a monoclinic $CoMoO_4$ phase (PDF#21-0868) to a cubic $CoMoO_3$ phase (PDF#21-0869), a cubic CoO phase (PDF#48-1719) and a Co_3O_4 phase after reduction. No metallic Co phase was noticed in the XRD of reduced MoO_3/CoO and $CoMoO_4$ catalysts. This phenomenon illustrates that Co species in MoO_3/CoO and $CoMoO_4$ are difficult to reduce. Moreover, we also found that the crystallinity of $CoMoO_4$ (14.7%) is lower than that of MoO_3/CoO (29%). This phenomenon indicates that abundant defect sites may exist on the surface of reduced $CoMoO_4$ catalyst.[25]

The XRD of other molybdate catalysts was analyzed. According to Fig. S2,† the $Fe_2(MoO_4)_3$ is mainly composed of a monoclinic $Fe_2(MoO_4)_3$ phase (PDF#35-0183). The $NiMoO_4$ exists in a monoclinic $NiMoO_4$ phase (PDF#33-0948). The $CuMoO_4$ is mainly composed of a triclinic $CuMoO_4$ phase (PDF#22-0242) and an orthorhombic $Cu_3Mo_2O_9$ phase (PDF#24-0055).

For comparison, we also prepared cobalt molybdate ($CoMoO_4$-X, X = Co/Mo atomic ratio) catalysts with different Co/Mo atomic ratios by the evaporation method. According to the XRD diffraction results illustrated in Fig. S3,† the cobalt molybdate catalysts are mainly composed of a monoclinic $CoMoO_4$ phase (PDF#21-0868).

The reducibility of the CoO, MoO_3, MoO_3/CoO and $CoMoO_4$ catalysts was analyzed by H_2-TPR. According to Fig. 7, a wide peak was found between 883 K and 1070 K in the H_2-TPR profile of the MoO_3 catalysts. According to the literature,[26] this peak was attributed to the partial reduction of MoO_3 to MoO_2. In the H_2-TPR profile of CoO, a wide peak was noticed at about 709 K. This peak can be assigned to the reduction of CoO to metallic Co.[27] In the TPR profile of MoO_3/CoO or $CoMoO_4$, a peak was observed at about 836 K. Compared with MoO_3, the MoO_3/CoO and $CoMoO_4$ catalysts are more reducible, which can be observed from the relatively low reduction temperatures in their H_2-TPR profiles. These results can be rationalized because the presence of Co species can promote the activation of H_2,[28] which is beneficial for the reduction of Mo^{6+} species.

Surface analysis of the reduced MoO_3, MoO_3/CoO and $CoMoO_4$ catalysts was carried out using X-ray photoelectron spectroscopy (XPS). The XPS survey spectra of reduced MoO_3, MoO_3/CoO and $CoMoO_4$ catalysts are illustrated in Fig. S4.† As we can see from Fig. 8, the coexistence of Mo^{6+}, Mo^{5+} and Mo^{6+} is evidenced by the Mo 3d XPS spectra of reduced MoO_3, MoO_3/CoO and $CoMoO_4$ catalysts. According to the literature,[4,29] the peaks at about 232.1 eV and 235.3 eV can be assigned to Mo^{6+} species, the peaks at 230.4 eV and 233.6 eV can be attributed to Mo^{5+} species, and the peaks at about 229.5 eV and 232.8 eV can be assigned to the Mo^{4+} species. The O 1s XPS spectra of reduced MoO_3, MoO_3/CoO and $CoMoO_4$ catalysts have two peaks at about 531.4 eV and 530.5 eV. The peaks at about 531.4 eV can be attributed to the surface oxygen species of catalysts that were adsorbed by the oxygen vacancies (O_{ads}).[30,31] The peaks at about 530.5 eV can be assigned to the lattice oxygen (O_{latt}). The percentages of the various Mo species (Mo^{6+}, Mo^{5+} and Mo^{4+}) and different O species (O_{latt} and O_{ads}) in the surface of reduced MoO_3, MoO_3/CoO and $CoMoO_4$ catalysts are shown in Fig. 9. The surface of reduced MoO_3 is mainly composed of Mo^{6+} (85.3%), accompanied by small amounts of Mo^{5+} (12.1%) and Mo^{4+} (2.6%). In contrast, the Mo species in the reduced MoO_3/CoO

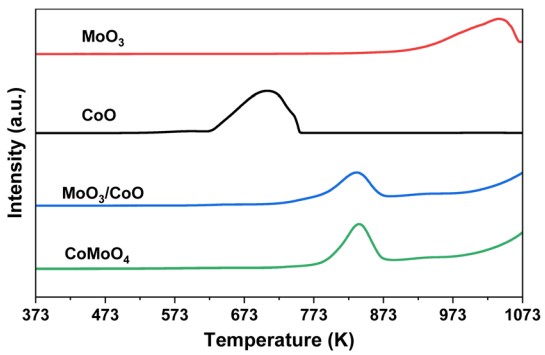

Fig. 7 H_2-TPR profiles of the MoO_3, CoO, MoO_3/CoO and $CoMoO_4$ catalysts.

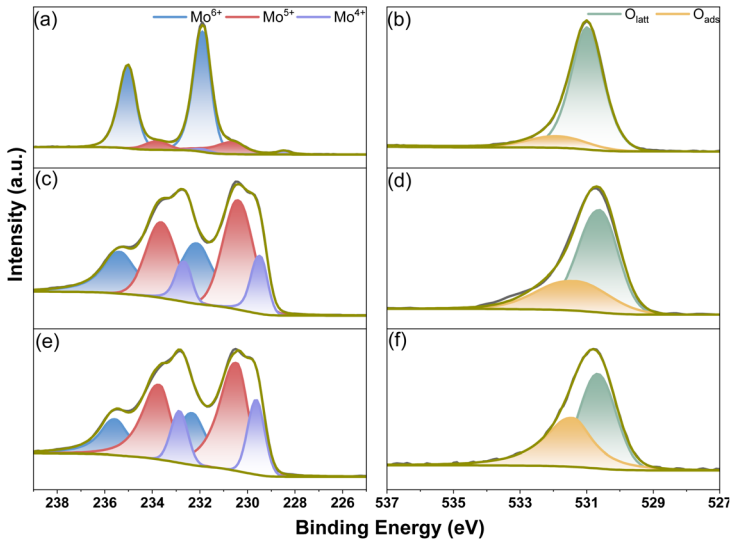

Fig. 8 XPS Mo 3d and O 1s core level spectra of the reduced (a and b) MoO_3, (c and d) MoO_3/CoO and (e and f) $CoMoO_4$ catalysts.

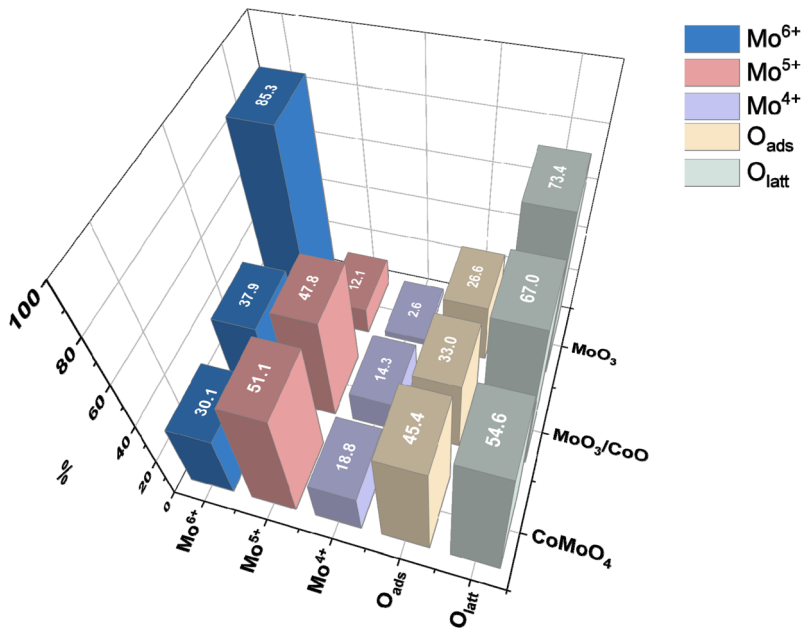

Fig. 9 The percentages of the various Mo species and O species on the reduced Mo-based catalysts.

is mainly composed of Mo^{5+} (47.8%), accompanied by Mo^{6+} (37.9%) and Mo^{4+} (14.3%). Compared with the reduced MoO_3 and MoO_3/CoO, the surface of a reduced $CoMoO_4$ catalyst has a higher proportion of Mo^{5+} (51.1%) and Mo^{4+} (18.5%). At the same time, it has a lower proportion of Mo^{6+} (30.1%). This phenomenon further confirms that the presence of Co species can facilitate the reduction of Mo^{6+} species to a low oxidation state of Mo species (Mo^{5+} and Mo^{4+}). According to the literature,[32] Mo^{5+} species can be considered as positively charged oxygen vacancies. Therefore, the reduced $CoMoO_4$ catalyst surface has more oxygen vacancies than MoO_3 and MoO_3/CoO. Based on the XPS results of O 1s, $CoMoO_4$ has a higher O_{ads} concentration (45.4%) than MoO_3 (26.6%) and MoO_3/CoO (33.0%). This result further confirms that the surface of the reduced $CoMoO_4$ catalyst has a higher oxygen vacancy concentration. According to Fig. S5,† Mo species mainly exist in the form of Mo^{6+} in the unreduced MoO_3, MoO_3/CoO and $CoMoO_4$ catalysts. This phenomenon further indicates that the presence of cobalt species can effectively promote the reduction of molybdenum species.

The oxygen vacancy concentrations of the reduced MoO_3, MoO_3/CoO and $CoMoO_4$ catalysts were measured by ultraviolet-visible (UV-Vis) diffuse reflectance spectroscopy (see Fig. 10).[33,34] Compared to reduced MoO_3, the reduced MoO_3/

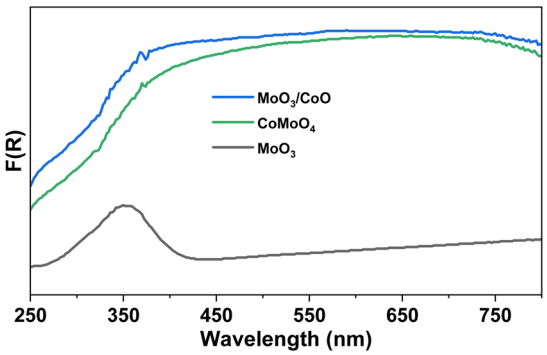

Fig. 10 UV–Vis spectra of the reduced MoO_3, MoO_3/CoO and $CoMoO_4$ catalysts.

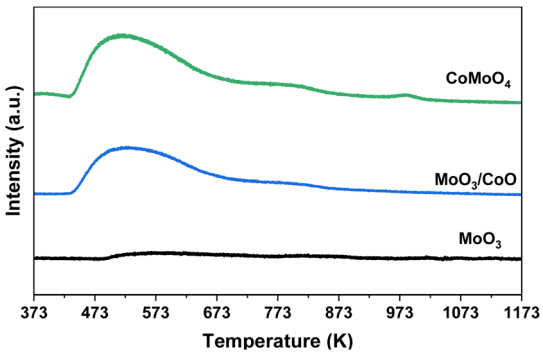

Fig. 12 NH_3-TPD profiles of the reduced MoO_3, MoO_3/CoO and $CoMoO_4$ catalysts.

CoO and $CoMoO_4$ catalysts exhibit stronger absorption in the wavelength range of 400–800 nm. This result indicates that the surfaces of MoO_3/CoO and $CoMoO_4$ catalysts contain more oxygen vacancies than that of MoO_3.[33] According to the literature,[35] there is some relationship between the edge energy (E_g) and the oxygen vacancy concentration of a catalyst. Generally, a catalyst with a lower E_g has a higher oxygen vacancy concentration. To compare the oxygen vacancy concentrations on the surfaces of the reduced MoO_3, MoO_3/CoO and $CoMoO_4$ catalysts, we also analyzed the E_g values of the reduced MoO_3, MoO_3/CoO and $CoMoO_4$ catalysts (see Fig. 11). Based on the E_g values of the reduced MoO_3 (3.01 eV), MoO_3/CoO (1.01 eV) and $CoMoO_4$ (0.82 eV) catalysts, the reduced $CoMoO_4$ has a higher oxygen vacancy concentration than the reduced MoO_3 and MoO_3/CoO catalysts.

The acidity (acid strength and the concentration of acid sites) of the reduced MoO_3, MoO_3/CoO and $CoMoO_4$ catalysts was analyzed using NH_3-TPD (see Fig. 12). The NH_3-TPD profile of the reduced MoO_3 catalyst shows no significant NH_3 desorption peak between 373 K and 1173 K. There is a broad NH_3 desorption peak around 518 K for the reduced MoO_3/CoO catalyst. The reduced $CoMoO_4$ catalyst exhibits three NH_3 desorption peaks at around 518 K, 820 K and 973 K, respectively. Compared to the reduced MoO_3 and MoO_3/CoO catalysts, the reduced $CoMoO_4$ exhibits NH_3 desorption peaks at higher temperatures, which means that the reduced $CoMoO_4$ catalyst has higher acid strength. From Table 2, we can see that the reduced $CoMoO_4$ catalyst also has higher acid concentration than the reduced MoO_3 and MoO_3/CoO. Based on the results of XPS and UV-Vis spectra, the reduced $CoMoO_4$ catalyst has higher oxygen vacancy concentration than the reduced MoO_3 and MoO_3/CoO catalysts. In some previous literature,[4,30,36] it has been suggested that the oxygen vacancies generated by partially reduced metal oxide catalysts can serve as Lewis acid sites. This may be the reason why the reduced $CoMoO_4$ catalyst has higher concentration of acid sites.

Table 2 The acid site concentrations of the investigated Mo-based catalysts (measured by NH_3-TPD)

Catalyst	Acid site concentration (mmol g^{-1})
MoO_3	0.096
MoO_3/CoO	0.543
$CoMoO_4$	1.450

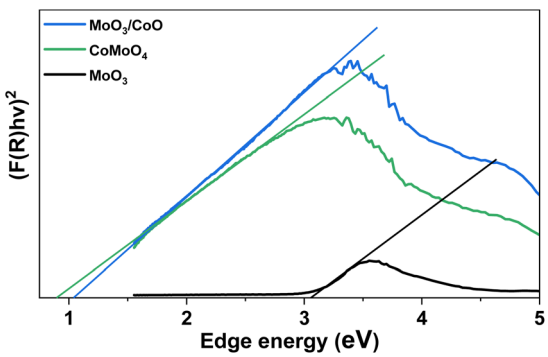

Fig. 11 Band gaps of the reduced MoO_3, MoO_3/CoO and $CoMoO_4$ catalysts.

Activity tests

As a representative of lignocellulosic ketones, 4-heptanone can be directly produced by the reaction of ABE fermentation products over tin-doped ceria catalysts.[16] Heptene is a C_7 olefin that can be used to manufacture aviation fuel by oligomerization and hydrogenation reactions. As the main purpose of this research work, we investigated the activity of CoO, MoO_3 + CoO, MoO_3, MoO_3/CoO and $CoMoO_4$ catalysts in the selective HDO of 4-heptone to heptene. According to the analysis of GC-MS (Fig. S6 and S7†), heptene was obtained as the only product. No heptane was detected in the products. The reaction pathway is shown in Scheme 1.

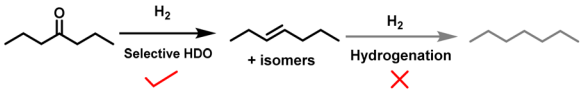

Scheme 1 Reaction pathway for the generation of heptene and heptane from the HDO of 4-heptanone.

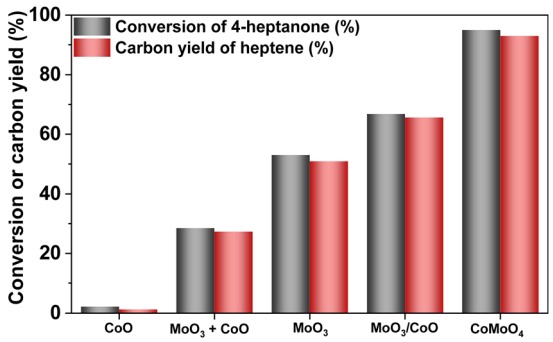

Fig. 13 Conversions of 4-heptanone and the carbon yields of heptene over the CoO, MoO_3 + CoO, MoO_3, MoO_3/CoO and $CoMoO_4$ catalysts. Reaction conditions: T = 673 K, P_{H_2} = 0.1 MPa, WHSV = 15 h^{-1}, initial H_2/4-heptanone molar ratio = 50 : 1.

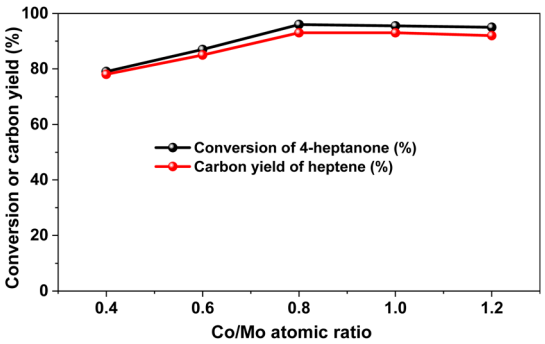

Fig. 14 Conversion of 4-heptanone and the carbon yield of heptene over the cobalt molybdate catalyst as a function of Co/Mo atomic ratio. Reaction conditions: T = 673 K, P_{H_2} = 0.1 MPa, WHSV = 15 h^{-1}, initial H_2/4-heptanone molar ratio = 50 : 1.

From Fig. 13, we can see that the CoO catalyst has low activity for the selective HDO of 4-heptanone to heptene. Different from CoO, the MoO_3 catalyst is active for the selective HDO of 4-heptanone to heptene. Moreover, a good 4-heptanone conversion (53%) and heptene carbon yield (51%) were achieved under the investigated reaction conditions. This is consistent with the previous work of Román-Leshkov *et al.* about similar reaction systems.[37] It is very interesting that the activity of MoO_3 was further improved after it was loaded on CoO. To understand this phenomenon, we studied the catalytic activity of MoO_3 + CoO prepared by physical mixing of MoO_3 and CoO at a Mo/Co atomic ratio of 1 : 1. It was found that the activity of MoO_3 + CoO was between those of the CoO and MoO_3. Based on these results, we believe that a close interaction of Co and Mo species is necessary for the higher activity of the MoO_3/CoO catalyst. To verify this speculation, we studied the activity of the $CoMoO_4$ catalyst prepared by the evaporation method. As we expected, evidently, a higher heptane conversion (95%) and heptene carbon yield (93%) were achieved over this catalyst under the investigated conditions.

For comparison, we also studied the catalytic performance of $Fe_2(MoO_4)_3$, $CuMoO_4$ and $NiMoO_4$ catalysts. From Fig. S8,† it could be found that the $CoMoO_4$ catalyst has better catalytic performance than other molybdates for the selective HDO of 4-heptanone to heptene. Moreover, an evident higher 4-heptanone conversion and a heptene carbon yield were achieved under the same reaction conditions.

The effects of the Co/Mo atomic ratio and reaction conditions on the catalytic performance of the $CoMoO_4$ catalyst were investigated (see Fig. 14–16). Under the optimal reaction conditions ($CoMoO_4$-0.8, T = 673 K, P_{H_2} = 0.1 MPa H_2, WHSV = 10 h^{-1}, initial H_2/4-heptanone molar ratio = 50 : 1), 98% 4-heptanone conversion and 96% heptene yield were achieved, respectively.

According to the characterization results, there are three reasons for the higher activity of the $CoMoO_4$ catalyst. (1) Higher BET specific surface area and good pore structure. According to the N_2-physisorption results (see Table 1), $CoMoO_4$ has a higher specific surface area and a larger pore volume and average pore size than CoO, MoO_3 and MoO_3/CoO. This can be considered as one of the reasons for its higher activity. (2) Higher concentration of oxygen vacancies (Mo^{5+}). According to previous literature reports,[37] the oxygen vacancies

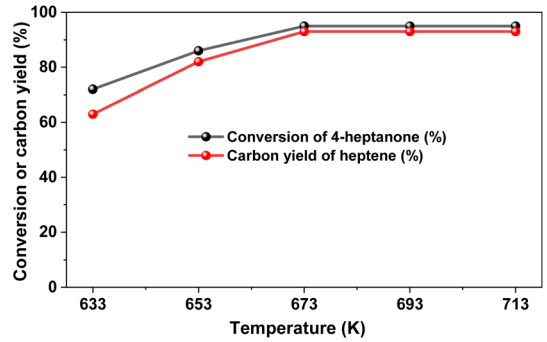

Fig. 15 Conversion of 4-heptanone and the carbon yield of heptene over the $CoMoO_4$-0.8 catalyst as a function of reaction temperature. Reaction conditions: P_{H_2} = 0.1 MPa, WHSV = 15 h^{-1}, initial H_2/4-heptanone molar ratio = 50 : 1.

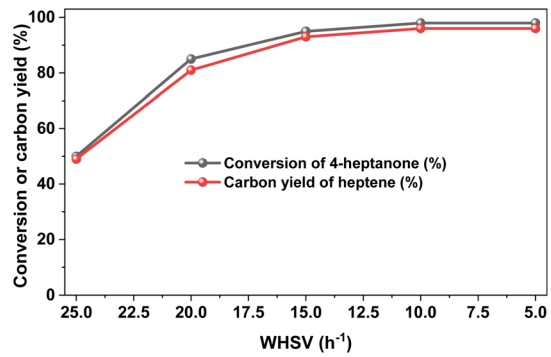

Fig. 16 Conversion of 4-heptanone and the carbon yield of heptene over the $CoMoO_4$-0.8 catalyst as a function of WHSV. Reaction conditions: T = 673 K, P_{H_2} = 0.1 MPa H_2, initial H_2/4-heptanone molar ratio = 50 : 1.

formed on the surface of a metal oxide by partial reduction can adsorb oxygenated organic compounds and convert oxygenated organic compounds into olefins by a deoxygenation reaction that follows a reversed Mars–van Krevelen mechanism (see Fig. 17). First, the $CoMoO_4$ catalyst is partially reduced by hydrogen and generates $CoMoO_3$ that contains oxygen vacancies (Mo^{5+}). Subsequently, the oxygen vacancies interact with the carbonyl oxygen of 4-heptanone and remove the carbonyl oxygen in the form of electron transfer to generate heptene. Finally, the catalyst is reduced by hydrogen and generates oxygen vacancies and H_2O. In the previous reports about a similar reaction system,[38] it has been suggested that the Mo^{5+} species (oxygen vacancies) produced by partially reducing MoO_3 is the active center for the selective HDO of biomass platform compounds. Based on the H_2-TPR, XPS and UV-Vis spectral results, the presence of Co species promotes the reduction of Mo species. As a result, more surface Mo^{5+} species (oxygen vacancies) are generated under the investigated conditions, which will lead to the high activity of $CoMoO_4$. To substantiate the significance of Mo^{5+} species (oxygen vacancy) in the selective HDO of 4-heptanone, a "H_2-OFF" experiment was carried out by switching the carrier gas from H_2 to N_2 during the selective HDO of 4-heptanone over the $CoMoO_4$ catalyst (see Fig. 18). As we expected, the 4-heptanone conversion and heptene carbon yield over the $CoMoO_4$ catalyst plummeted within 60 minutes. After we switched back the carrier gas to H_2, the catalytic activity of $CoMoO_4$ was slowly restored. This result indicated that the selective HDO reaction was catalyzed by the Mo^{5+} species (oxygen vacancy) generated through *in situ* reduction of H_2. (3) Stronger acidity and higher acid site concentration. The NH_3-TPD results reveal that the reduced $CoMoO_4$ catalyst exhibits higher acid strength and higher acid site concentration than other catalysts. Based on the literature,[39] the Lewis acid site of a metal oxide can interact with a lone pair of oxygen atoms and weaken the energy of C–O bonds. Therefore, the higher acid strength and higher acid concentration of the reduced $CoMoO_4$ catalyst are more conducive to the selective HDO reaction.

For the practical application, the stability of $CoMoO_4$-0.8 for the selective HDO of 4-heptanone to heptane was investigated under a relatively high WHSV (20 h^{-1}). As shown in Fig. 19, the

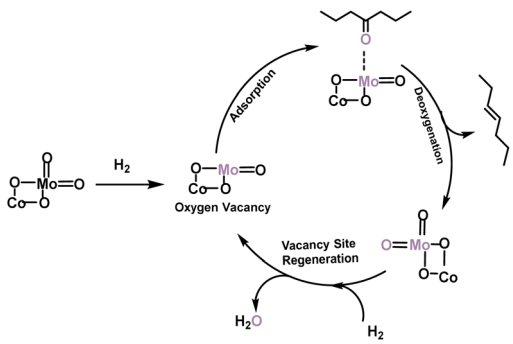

Fig. 17 Reaction mechanism for the selective HDO of 4-heptanone to heptene over the $CoMoO_4$ catalyst.

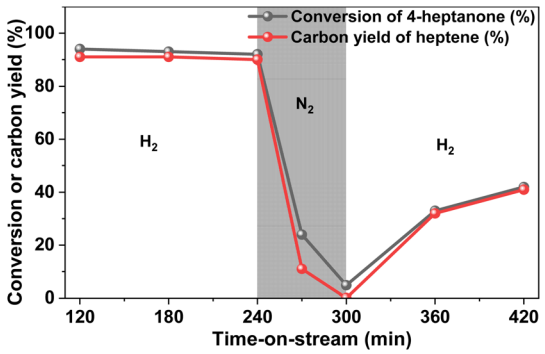

Fig. 18 Conversion of 4-heptanone and the carbon yield of heptene over the $CoMoO_4$-0.8 catalyst as a function of time-on-steam under a H_2 (or N_2) atmosphere. Reaction conditions: T = 673 K, P_{H_2} = 0.1 MPa H_2, WHSV = 14 h^{-1}, initial H_2 (or N_2)/4-heptanone molar ratio = 50 : 1.

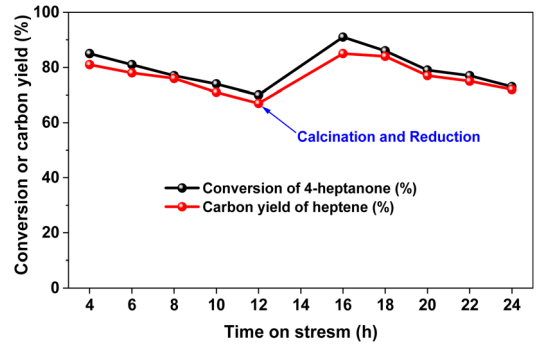

Fig. 19 Conversion of 4-heptanone and the carbon yield of heptene over $CoMoO_4$-0.8 as a function of time-on-stream. Reaction conditions: T = 673 K, P_{H_2} = 0.1 MPa, WHSV = 20 h^{-1}, initial H_2/4-heptanone molar ratio = 50 : 1.

4-heptanone conversion and heptene carbon yield decrease with the reaction time. However, such a problem can be solved by regeneration. After being calcined at 673 K under air flow for 1 h and reduced at 673 K under H_2 flow for 1 h, the activity of the $CoMoO_4$-0.8 catalyst was restored to its initial value. Based on this result, we think that the decreased catalyst activity of $CoMoO_4$-0.8 may be caused by a carbon deposit generated on the catalyst surface under high WHSV. To verify this, we characterized the fresh and spent $CoMoO_4$-0.8 catalysts by TG-MS. According to Fig. S9,† about 10% weight increase was observed at 400 K–720 K in the TG-MS profile of the fresh $CoMoO_4$-0.8 catalyst. This phenomenon can be explained by the oxidation of the catalyst. No CO_2 was generated at 300 K–900 K. From Fig. S10,† about 4% weight loss was observed at 650 K–800 K in the TG-MS profile of spent $CoMoO_4$-0.8. Meanwhile, CO_2 was detected in the gaseous product. These results indicate that carbon deposition has occurred on the surface of the catalyst during stability testing, which may be the reason for catalyst deactivation.

The applicability of the $CoMoO_4$-0.8 catalyst for the selective HDO of other lignocellulosic ketones to olefins was checked as

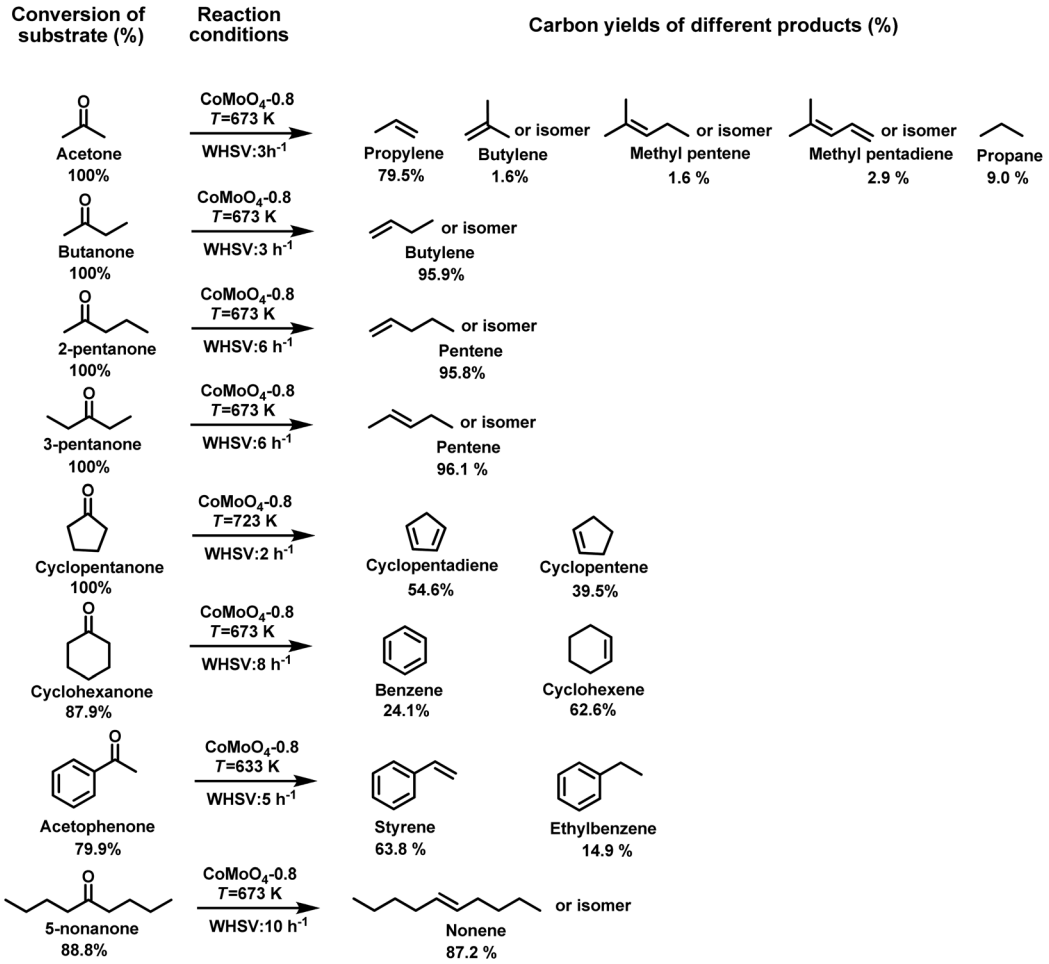

Fig. 20 Conversions of lignocellulosic ketones and the carbon yields of different products over the $CoMoO_4$-0.8 catalyst.

well. As shown in Fig. 20 and Fig. S11–S29 in the ESI,† the selective HDO of acetone, butanone, 2-pentanone, 3-pentanone, cyclopentanone, cyclohexanone, 5-nonanone and acetophenone over the $CoMoO_4$-0.8 catalyst led to high carbon yields of the corresponding olefins (propylene, butene, pentene, cyclopentene, cyclopentadiene, cyclohexene, styrene and nonene) under similar reaction conditions to those we used for 4-heptanone. These olefins can be used as feedstocks in the production of polymers, diesel fuel, aviation fuel, *etc*. For example, propylene is an important feedstock in the production of fuels, rubber, plastics, synthetic fibers, medicines, *etc*.[40] Butene can not only be used to synthesize rubber and plastics by polymerization reactions, but also be used to manufacture aviation fuel by oligomerization reactions followed by hydrogenation.[41] Styrene, as a significant chemical, is widely used to synthesize plastics, resins, coatings, medicines, *etc*.[42] As another potential application, $CoMoO_4$-0.8 also shows good catalytic performance in the selective HDO of lignin-derived aryl ethers (such as anisole and guaiacol)[43] to aromatics (Fig. S30–S34†). It is worth mentioning that some alkylated benzenes were also obtained at the same time. These products may be generated by the alkylation of benzene (theoretical HDO product) with methanol over the acid sites on the surface of the $CoMoO_4$-0.8 catalyst. Taking into consideration the eco-friendly and simple preparation method, high activity, good selectivity, regenerability and universality of the $CoMoO_4$-0.8 catalyst, we believe it can be considered as a promising catalyst in future applications.

Conclusions

In summary, the cobalt molybdate ($CoMoO_4$) catalyst manufactured by an eco-friendly and simple evaporation method demonstrated outstanding performance for the selective HDO of lignocellulose-derived ketones to olefins. Moreover, a high 4-heptanone conversion (98%) and a good carbon yield (96%) of heptene were achieved under the optimal conditions. According to the characterization results, the remarkable catalytic performance of $CoMoO_4$ is ascribed to its larger specific surface area, good pore structure, higher oxygen vacancy (Mo^{5+} species) concentration, higher acid strength and higher acid site concentration compared with the other investigated catalysts. Furthermore, the $CoMoO_4$ catalyst is also applicable for

the selective HDO of other lignocellulose-derived ketones (such as acetone, butanone, 2-pentanone, 3-pentanone, cyclopentanone, cyclohexanone, 5-nonanone and acetophenone) to their corresponding olefins (propylene, butene, pentene, cyclopentene, cyclopentadiene, cyclohexene, styrene and nonene). These olefins can be used as feedstocks in the production of fuels, lubricants, drugs, cosmetics, polymers, coatings, surfactants, detergents, *etc*. Considering its eco-friendly and simple preparation method, high activity and selectivity, good regenerability and applicability, the $CoMoO_4$ catalyst has a good application prospect for the manufacture of olefins with lignocellulose-derived ketones.

Conflicts of interest

There are no conflicts to declare.

Acknowledgements

This work was supported by the National Key R&D Program of China (no. 2022YFB4201802) and the National Natural Science Foundation of China (no. 21721004, 22178335 and 22078318).

References

1 T. Zhang, *Science*, 2020, **367**, 1305; T. P. Vispute, H. Zhang, A. Sanna, R. Xiao and G. W. Huber, *Science*, 2010, **330**, 1222; A. J. Ragauskas, G. T. Beckham, M. J. Biddy, R. Chandra, F. Chen, M. F. Davis, B. H. Davison, R. A. Dixon, P. Gilna, M. Keller, P. Langan, A. K. Naskar, J. N. Saddler, T. J. Tschaplinski, G. A. Tuskan and C. E. Wyman, *Science*, 2014, **344**, 1246843; K. Sanderson, *Nature*, 2011, **474**, S12.

2 P. Anbarasan, Z. C. Baer, S. Sreekumar, E. Gross, J. B. Binder, H. W. Blanch, D. S. Clark and F. D. Toste, *Nature*, 2012, **491**, 235.

3 J. Q. Bond, D. M. Alonso, D. Wang, R. M. West and J. A. Dumesic, *Science*, 2010, **327**, 1110; G. W. Huber, J. N. Chheda, C. J. Barrett and J. A. Dumesic, *Science*, 2005, **308**, 1446; G. W. Huber, S. Iborra and A. Corma, *Chem. Rev.*, 2006, **106**, 4044; Y. Liu, Y. Nie, X. Lu, X. Zhang, H. He, F. Pan, L. Zhou, X. Liu, X. Ji and S. Zhang, *Green Chem.*, 2019, **21**, 3499; X. Wu, N. Luo, S. Xie, H. Zhang, Q. Zhang, F. Wang and Y. Wang, *Chem. Soc. Rev.*, 2020, **49**, 6198; H. Zhou, M. Wang and F. Wang, *Joule*, 2021, **5**, 3031; S. Wang, A. Cheng, F. Liu, J. Zhang, T. Xia, X. Zeng, W. Fan and Y. Zhang, *Ind. Chem. Mater.*, 2023, **1**, 188; X. Tong, P. Guo, S. Liao, S. Xue and H. Zhang, *Green Chem.*, 2019, **21**, 5828.

4 F. Han, Y. Liu, G. Li, L. Yuan, A. Wang, F. Wang, T. Zhang and N. Li, *Green Chem.*, 2023, **25**, 1056.

5 B. G. Harvey and R. L. Quintana, *Energy Environ. Sci.*, 2010, **3**, 352; J. A. Martens, W. H. Verrelst, G. M. Mathys, S. H. Brown and P. A. Jacobs, *Angew. Chem., Int. Ed.*, 2005, **44**, 5687; Z. Xu, J. P. Chada, D. Zhao, C. A. Carrero, Y. T. Kim, D. C. Rosenfeld, J. L. Rogers, S. J. Rozeveld, I. Hermans and G. W. Huber, *ACS Catal.*, 2016, **6**, 3815; H. Zhang, Y.-T. Cheng, T. P. Vispute, R. Xiao and G. W. Huber, *Energy Environ. Sci.*, 2011, **4**, 2297; M. A. Ershov, V. D. Savelenko, U. A. Makhova, V. M. Kapustin, T. M. M. Abdellatief, N. V. Karpov, E. V. Dutlov and D. V. Borisanov, *Fuel*, 2022, **321**, 124016; Y. Peng, M. Dong, X. Meng, B. Zong and J. Zhang, *AIChE J.*, 2009, **55**, 717.

6 V. P. Doronin, O. V. Potapenko, T. P. Sorokina, P. V. Lipin, K. I. Dmitriev, K. S. Plekhova, D. O. Kondrashev and A. V. Kleimenov, *Catal. Today*, 2021, **378**, 75; A. Y. Borisevich, S. Wang, S. N. Rashkeev, M. Glazoff, S. J. Pennycook and S. T. Pantelides, *Adv. Mater.*, 2007, **19**, 2129; Y. Xu, X. Li and M. Ding, *Chem*, 2021, **7**, 1977.

7 Z. Zhao, J. Jiang and F. Wang, *J. Energy Chem.*, 2021, **56**, 193.

8 H. Luo, L. Ge, J. Zhang, J. Ding, R. Chen and Z. Shi, *Bioresour. Technol.*, 2016, **200**, 111; M. I. Piñón-Muñiz, V. H. Ramos-Sánchez, N. Gutiérrez-Méndez, S. B. Pérez-Vega, J. C. Sacramento-Rivero, C. I. Vargas-Consuelos, F. M. Martinez, O. A. Graeve, R. E. Orozco-Mena, A. Quintero-Ramos, M. A. Sánchez-Madrigal and I. Salmerón, *Renewable Energy*, 2023, **212**, 632; K. Sandesh, R. K. Shishir and C. Vaman Rao, *Fuel*, 2020, **262**, 116499.

9 T. N. Pham, T. Sooknoi, S. P. Crossley and D. E. Resasco, *ACS Catal.*, 2013, **3**, 2456; R. Xing, W. Qi and G. W. Huber, *Energy Environ. Sci.*, 2011, **4**, 2193.

10 K. Min, S. Kim, T. Yum, Y. Kim, B.-I. Sang and Y. Um, *Appl. Microbiol. Biotechnol.*, 2013, **97**, 5627; C. R. Mehrer, J. M. Rand, M. R. Incha, T. B. Cook, B. Demir, A. H. Motagamwala, D. Kim, J. A. Dumesic and B. F. Pfleger, *Metab. Eng.*, 2019, **55**, 92.

11 G. Singh, T. S. Khan, C. Samanta, R. Bal and A. Bordoloi, *Biomass Bioenergy*, 2022, **156**, 106321.

12 J. C. Serrano-Ruiz and J. A. Dumesic, *ChemSusChem*, 2009, **2**, 581.

13 Y. L. Wang, W. P. Deng, B. J. Wang, Q. H. Zhang, X. Y. Wan, Z. C. Tang, Y. Wang, C. Zhu, Z. X. Cao, G. C. Wang and H. L. Wan, *Nat. Commun.*, 2013, **4**, 2141.

14 Z. Hu, A. Xie, C. Chen, Z. Zou, Y. Shen, Z. Fu, Y. Zhang, H. Zhang, H. Zhao and G. Wang, *Fuel*, 2022, **319**, 123815; X. Gao, Y. Ding, L. Peng, D. Yang, X. Wan, C. Zhou, W. Liu, Y. Dai and Y. Yang, *Fuel*, 2022, **314**, 123074; M. Dohade and P. L. Dhepe, *Catal. Sci. Technol.*, 2018, **8**, 5259.

15 H. Zhou, B. Han, T. Liu, X. Zhong, G. Zhuang and J. Wang, *Green Chem.*, 2017, **19**, 3585; H. Jiang, Z. Qu, Y. Liu, X. Liu, G. Wang, Y. Wang, L. Xu, K. Ding, W. Xing and R. Chen, *Ind. Eng. Chem. Res.*, 2020, **59**, 13848.

16 Y. Wang, M. Peng, J. Zhang, Z. Zhang, J. An, S. Du, H. An, F. Fan, X. Liu, P. Zhai, D. Ma and F. Wang, *Nat. Commun.*, 2018, **9**, 5183.

17 A. D. Patel, J. C. Serrano-Ruiz, J. A. Dumesic and R. P. Anex, *Chem. Eng. J.*, 2010, **160**, 311; J. C. Serrano-Ruiz, D. J. Braden, R. M. West and J. A. Dumesic, *Appl. Catal., B*, 2010, **100**, 184.

18 H.-M. Yang, W. Zhao, K. Norinaga, J.-J. Fang, Y.-G. Wang, Z.-M. Zong and X.-Y. Wei, *Sep. Purif. Technol.*, 2015, **152**, 238; A. Undri, M. Abou-Zaid, C. Briens, F. Berruti, L. Rosi, M. Bartoli, M. Frediani and P. Frediani, *J. Anal. Appl. Pyrolysis*, 2015, **114**, 208; Q. Yu, Z. Song, X. Chen, J. Fan, J. H. Clark, Z. Wang, Y. Sun and Z. Yuan, *Green Chem.*, 2020, **22**, 6415.

19 K. Wang, Y. Li, J. Hu, Z. Lu, J. Xie, A. Hao and Y. Cao, *Chem. Eng. J.*, 2022, **447**, 137540.

20 M. Li, S. Xu, C. Cherry, Y. Zhu, D. Wu, C. Zhang, X. Zhang, R. Huang, R. Qi, L. Wang and P. K. Chu, *J. Mater. Chem. A*, 2015, **3**, 13776.

21 J. Zhou, S. Deng, L. Liu, Y. Lan and C. Chen, *Chem. Eng. J.*, 2023, **451**, 138754.

22 S. Chen, J. Wu, G. Wang, J. Wang, L. Fan, J. Hao, S. Wang, Y. Liu, H. Wu, Y. Li, J. Gao and M. Yang, *Coatings*, 2022, **12**, 1771.

23 I. Kashif, A. A. Soliman and Z. M. El-Bahy, *J. Alloys Compd.*, 2008, **452**, 384.

24 Y. Liu, R. Wang, H. Qi, X. Y. Liu, G. Li, A. Wang, X. Wang, Y. Cong, T. Zhang and N. Li, *Nat. Commun.*, 2021, **12**, 46.

25 X. Liu, J. Meng, J. Zhu, M. Huang, B. Wen, R. Guo and L. Mai, *Adv. Mater.*, 2021, **33**, 2007344; P. Wang, X. Ma, X. Hao, B. Tang, A. Abudula and G. Guan, *Catal. Rev.*, 2022, 1.

26 P. Novotný, S. Yusuf, F. Li and H. H. Lamb, *Catal. Today*, 2018, **317**, 50.

27 Y. Ji, Z. Zhao, A. Duan, G. Jiang and J. Liu, *J. Phys. Chem. C*, 2009, **113**, 7186.

28 S. Xiang, L. Dong, Z.-Q. Wang, X. Han, L. L. Daemen, J. Li, Y. Cheng, Y. Guo, X. Liu, Y. Hu, A. J. Ramirez-Cuesta, S. Yang, X.-Q. Gong and Y. Wang, *Nat. Commun.*, 2022, **13**, 3657; H. Zhang, X. Zhou, L. Liu, F. Lan, T. Zhao, M. Qiu, Q. Guan and W. Li, *Appl. Catal., B*, 2023, **338**, 123026; H. Wang, S. Bai, Y. Pi, Q. Shao, Y. Tan and X. Huang, *ACS Catal.*, 2019, **9**, 154.

29 M. Vasilopoulou, A. M. Douvas, D. G. Georgiadou, L. C. Palilis, S. Kennou, L. Sygellou, A. Soultati, I. Kostis, G. Papadimitropoulos, D. Davazoglou and P. Argitis, *J. Am. Chem. Soc.*, 2012, **134**, 16178.

30 Q. Deng, R. Gao, X. Li, J. Wang, Z. Zeng, J.-J. Zou and S. Deng, *ACS Catal.*, 2020, **10**, 7355.

31 S. Jaiswar and K. D. Mandal, *J. Phys. Chem. C*, 2017, **121**, 19586; P. Wang, X. Li, S. Fan, X. Chen, M. Qin, D. Long, M. O. Tadé and S. Liu, *Appl. Catal., B*, 2020, **279**, 119340.

32 O. Ambriz-Peláez, S. Durón, A. Olivas, R. Valdez, L. G. Arriaga, L. Álvarez-Contreras, M. Guerra-Balcázar and N. Arjona, *Appl. Surf. Sci.*, 2019, **498**, 143842.

33 J. Li, M. Zhang, Z. Guan, Q. Li, C. He and J. Yang, *Appl. Catal., B*, 2017, **206**, 300.

34 I. M. Szilágyi, B. Fórizs, O. Rosseler, Á. Szegedi, P. Németh, P. Király, G. Tárkányi, B. Vajna, K. Varga-Josepovits, K. László, A. L. Tóth, P. Baranyai and M. Leskelä, *J. Catal.*, 2012, **294**, 119.

35 S. Huang, R. Bao, J. Wang, J. Yi, Z. Zhang, L. Liu, Y. Han, Z. Li, D. Min, W. Zhang, Z. Ge and X. Zhang, *J. Alloys Compd.*, 2023, **961**, 170945; J. Nie, X. Yu, Z. Liu, J. Zhang, Y. Ma, Y. Chen, Q. Ji, N. Zhao and Z. Chang, *J. Cleaner Prod.*, 2022, **363**, 132593.

36 L. Wen, X. Li, R. Zhang, H. Liang, Q. Zhang, C. Su and Y.-J. Zeng, *ACS Appl. Mater. Interfaces*, 2021, **13**, 14181; X. Wang, L. Lu, B. Wang, Z. Xu, Z. Xin, S. Yan, Z. Geng and Z. Zou, *Adv. Funct. Mater.*, 2018, **28**, 1804191; J. Qi, S. Zhou, K. Xie and S. Lin, *J. Energy Chem.*, 2021, **60**, 249.

37 T. Prasomsri, T. Nimmanwudipong and Y. Román-Leshkov, *Energy Environ. Sci.*, 2013, **6**, 1732.

38 T. Prasomsri, M. Shetty, K. Murugappan and Y. Román-Leshkov, *Energy Environ. Sci.*, 2014, **7**, 2660.

39 M. Zhao, K. Yuan, Y. Wang, G. Li, J. Guo, L. Gu, W. Hu, H. Zhao and Z. Tang, *Nature*, 2016, **539**, 76.

40 W. Wang, S. Chen, C. Pei, R. Luo, J. Sun, H. Song, G. Sun, X. Wang, Z.-J. Zhao and J. Gong, *Science*, 2023, **318**, 886.

41 M. M. Bhasin, J. H. McCain, B. V. Vora, T. Imai and P. R. Pujadó, *Appl. Catal., A*, 2001, **221**, 397; H. Kim, D. Kim, Y.-K. Park and J.-K. Jeon, *Res. Chem. Intermed.*, 2018, **44**, 3823.

42 M. Ghadiri, A. Hemmati and M. Rezakazemi, *Int. J. Hydrogen Energy*, 2021, **46**, 28641.

43 J. Zakzeski, P. C. A. Bruijnincx, A. L. Jongerius and B. M. Weckhuysen, *Chem. Rev.*, 2010, **110**, 3552.